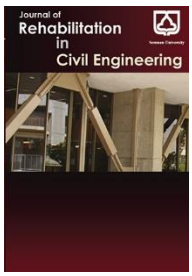

Journal homepage: http://civiljournal.semnan.ac.ir/

Calibration of Bar-Concrete Bond Stress Relationships for Bond Stress Prediction of GFRP Soil Nails Using Experimental Pullout Tests

B. Hamedmirjafari[1], J. Bolouri Bazaz[2*] and S. Abrishami[3]

1. Ph.D. Candidate, Department of Civil Engineering, Ferdowsi University of Mashhad, Mashhad, Iran.
2. Associate Professor, Department of Civil Engineering, Ferdowsi University of Mashhad, Mashhad, Iran.
3. Assistant Professor, Department of Civil Engineering, Ferdowsi University of Mashhad, Mashhad, Iran.

* Corresponding author: bolouri@um.ac.ir

ARTICLE INFO

Article history:
Received: 01 June 2018
Accepted: 19 April 2019

Keywords:
GFRP Soil Nail,
Bond Stress Model,
Statistical Criteria,
Pullout Test,
Calibration.

ABSTRACT

Even though steel bar is a conventional reinforcement in soil stabilization systems, the problem of corrosion of steel may lead to vast damages especially in aggressive environments. In the past decades, Fiber Reinforced Polymer (FRP) materials have offered an effective solution to overcome the corrosion problem. Despite numerous bond stress-displacement models for reinforcements in concrete, there is a lack of models for FRP nails in grout. In this paper, the usability of four bond stress models (Malvar, EPB, CMR and Soroushian) of reinforcements in concrete was evaluated to predict the bond stress of FRP nails in grout. For this purpose, the results of several experimental pullout tests were used to calibrate the reinforcement-concrete bond stress models and the constant parameters were obtained. To evaluate the accuracy of the calibrated models, four statistical criteria of R2, SSE, RMSE and MAPE have been also determined for each model. Results showed that Malvar model with R2 of 0.94 and MAPE of %21 was deemed suitable for the prediction of bond stress of GFRP nails while CMR model is not recommended.

1. Introduction

In the past decades, fiber-reinforced polymers (FRPs) have been increasingly used because of their overall performance of light weight, high tensile strength, high durability, low cost and corrosion resistance, and they have received growing attention as reinforcement in concrete structures or embedded in grout [1]. The use of conventional reinforcement materials in civil engineering may lead to certain shortcomings. For instance, steel reinforcements have corrosion risks in aggressive soil environments. FRP materials with high advantages are able to eliminate the corrosion problem in comparison with steel [2].

In the literature, some researchers focused on the determination of bond stress between various types of FRP bars and concrete under different conditions [1, 3-

DOI: 10.22075/JRCE.2019.14856.1279

6]. Moreover, bond stress depends on the arrangement of FRP bars [7-9] and concrete characteristics were taken into consideration [10-13]. Besides this, the flexural strength of concrete members reinforced with different types of FRP bars was evaluated as well [14-20].

Furthermore, bond stress at the interface between steel bar and concrete has been explored in different conditions including different types of bars [21-23], different types of concrete [24-28] and an analytical bond stress–displacement relationship has been developed [29]. Given that corrosion is so effective on bar-concrete bond stress, an experimental study [30] and three new models have been developed to predict the bond stress-displacement relationship of steel bar in concrete involving different types of steel corrosion [31]. Numerous studies have been conducted to compare the bond stress at the interface of steel, FRP and hybrid FRP-steel bars with surrounding concrete [32-34].

Other investigations have reserched the bond stress between steel reinforcement and cement grout in order to obtain the ultimate pullout load [35-38] and effective parameters were also investigated [39,40]. However, less attention have been paid to experimental, analytical or numerical models to predict the bond stress of FRP nails in cement grout and the comparison of the behavior of that with steel nails [41-45].

Nail-grout bond stress is the main design parameter in soil stabilization systems including soil nailing and micropile among others. It is, therefore, essential to investigate the bond stress of FRP nails in cement grout as an alternative for steel nail. Numerous bond stress models for steel or GFRP bars in concrete have been introduced so far, but a lack of bond stress models for GFRP nails in grout is strongly felt. Therefore, the evaluation of the usability of the bond stress models of concrete reinforcements to predict the bond stress of FRP nails in cement grout is essential, which has inspired the authors to conduct this research.

In 1983, a simple analytical model was proposed for the prediction of bond strength and displacement of steel bars in concrete which was known as the EPB model [23]. In 1989, local bond stress at the steel bar-concrete interface was investigated and a bond stress-displacement relationship was introduced [22]. In 1994, the first model to predict the relationship between bond stress and displacement of FRP bars in concrete was proposed [46]. Next model to predict the bond stress and displacement of FRP bar as concrete reinforcement was developed in 1995 and became well-known as the CMR model [47].

In this paper, four bond stress models of bar-concrete interface, including Malvar, EPB, CMR and Soroushian, were calibrated by experimental pullout tests to estimate the bond stress of GFRP nails. To ensure the accuracy of the results, four statistical criteria including square of the correlation coefficient (R^2), sum of squared errors (SSE), root-mean-square error (RMSE) and mean absolute percentage error (MAPE) have been determined for each calibrated model and the best performance model was suggested.

Findings indicated that Malvar with R^2 of 0.94, MAPE of 21%, SSE of 0.32 and RMSE of 0.07 is the best fitted model for GFRP nails while CMR with R^2 of 0.84 and MAPE of 42% is not suitable for GFRP nails.

2. Reinforcement-Concrete Bond Stress Models

Different bond stress-displacement models have been proposed in the literature which describe the bond stress between reinforcements and concrete. However, the models to predict bond stress between FRP nails and cement grout are rare. The following sections briefly describe the details of the bond stress-displacement models.

2.1 Malvar's Model

In 1994, Malvar proposed the first bond stress-displacement model of concrete embedded FRP bars. The model was derived from some experimental pullout tests of GFRP bars in concrete. In the proposed model, the effect of different values of concrete tensile strength and confining pressure on the pullout load was also considered. Eq. (1) describes the bond stress-displacement model which is dependent on two empirical constant parameters.

$$\tau = \tau_m . \frac{F.\frac{\delta}{\delta m}+(G-1).(\frac{\delta}{\delta m})^2}{1+(F-2).\frac{\delta}{\delta m}+G.(\frac{\delta}{\delta m})^2} \quad (1)$$

In this equation τ, δ, τ_m, and δ_m are bond stress, displacement at any state, peak bond stress and the corresponding displacement at the peak, respectively. F and G are constant parameters which may be found by the experimental pullout test results.

Original model developers, as an example, calibrated the model based on some experimental pullout tests in two different conditions. The parameter of F was calibrated to 11.0 and 13.0, while G was calibrated to 1.2 and 0.5 [46].

2.2 EPB Model (Eligehausen, Popov, and Bertero)

In 1982, Eligehausen, Popov and Bertero reported a comprehensive research on bond stress-displacement models of steel reinforcing bars in concrete. By conducting 125 pullout tests, effects of different parameters such as the bar type and diameter, confinement pressure and compressive strength of concrete on the bond strength were examined. Different types of loading such as monotonic and cyclic, have been evaluated. Finally, based on the results of the experimental tests, a simple analytical model for the prediction of bond strength and displacement of steel bars in concrete were proposed. The main purpose of the research was to predict the bond strength of steel bar in concrete in beam-column joints. Therefore, different types of cyclic loading were tested as representative of the earthquake loading. The model which has been verified by the experimental tests is now so popular and is called EPB model. Eq. (2) describes the ascending segment of the EPB analytical model of bond stress-displacement [23].

$$\frac{\tau}{\tau_1} = \left(\frac{S}{S_1}\right)^{\alpha} \quad (2)$$

Where α is the empirical constant parameter which could be found by using experimental pullout tests. τ_1 is the peak bond stress and S_1 is the corresponding displacement at the peak bond stress. τ and S are the bond stress and displacement at any state, respectively.

Original model developers, as an example, calibrated the model by using some pullout tests of steel rebar in concrete. The parameter of α was found to be 0.33 and 0.45 in two different patterns of stress and certain properties of concrete [23].

2.3 Soroushian and Choi's Model

In 1989, Soroushian and Choi investigated the local bond stress of concrete embedded steel bars. The research addressed the effects of bar diameters on the bond stress-displacement relationship. Experimental data of deformed bars which were partially embedded in concrete were used to evaluate the ultimate local bond strength and the local bond stress-displacement relationship in confined concrete [39]. The proposed bond stress-displacement relationship is given by Eq. (3) [22].

$$\tau = \tau_{max}(S/S_1).\exp(1-(S/^{[1-(S/S_1)^{\alpha}]} \quad (3)$$

In Eq. (5), τ_{max} and S_1 are the ultimate bond stress and displacement at the top of the bond stress-displacement curve, while τ and S are bond stress and displacement at any location of the curve, respectively. Parameter α is constant and could be obtained using experimental tests [22].

In 1991, Soroushian modified the bond stress-displacement model by taking into account the effects of confinement and compressive strength of concrete. The modified model showed that the confining pressure effect on bond stress is negligible. Eq. (4) describes the modified Soroushian's bond stress-displacement model [28].

$$\tau = \tau_{max}(S/S_1).e^{[1-(S/S_1)^{\alpha}]/\alpha} \quad (4)$$

The original model developers did not calibrate their model with any example of actual tests and no range of values was presented.

2.4 CMR Model

Cosenza, Manfredi and Realfonzo in 1995 presented a bond stress-displacement model named "CMR" model. The model was derived from the already proposed EPB model to predict the bond stress-displacement relationship of FRP bars in concrete. The main expression of CMR model is shown by Eq. (5) [47].

$$\frac{\tau}{\tau_m} = (1 - e^{\frac{-s}{sr}})^{\alpha} \quad (5)$$

Where τ_m and S_r are the peak bond stress and displacement, respectively. The displacement and bond stress at any point on the curve have been signified by τ and S, respectively. Also, α is a constant parameter which can be found by the calibration of the relationship with the actual data.

By using some examples of actual pullout tests, the value of the parameter α was proposed as a range between 0.16 and 1.49, which is heavily dependent on the properties of the reinforcement and concrete [47].

3. Experimental Pullout Tests

Two different series of pullout tests have been carried out. The first series include GFRP bar in cement grout without soil surcharge and the second series contains pullout tests in the soil box.

3.1 Tests without Soil Surcharge (the First Series)

The first series of pullout tests consist of twelve specimens which were prepared with no surrounding soil. These series of tests include different water cement ratios of grout at various embedded lengths. To evaluate the bond stress between nails and grout, some specimens were prepared in the laboratory. A GFRP bar was axially installed inside a PVC pipe and was carefully made stable at the center of the pipe with the aid of some centralizers. The pipe was then filled with cement grout gravitationally, i.e. no injection pressure was used. In all the specimens, the reinforcing bar was longer than the PVC pipe, extended backward and forward. The extension was needed to locate tension and

measurement equipment. Pullout load was applied with a hydraulic jack. Load cell and LVDT were used to measure and record the load and displacement.

In each test, three cubic samples of grout were taken and the compressive strength (f'_c) of samples was measured after seven days of grouting. Table 1 summarizes the specifications of all specimens.

The pullout test apparatus was made up of a main steel board, which was fixed using a horizontal support for a rigid frame and vertical support for the rigid reinforced concrete ground. The pullout test apparatus with the components is shown in Fig. 1 schematically.

Table 1. Tests without Soil Surcharge.

Test No.	W/C	f'c (kN/m2)	L (mm)
1	0.5	21020	50
2	0.5	21020	100
3	0.5	21020	150
4	0.5	21020	200
5	0.5	21020	250
6	0.5	21020	400
7	0.5	21020	600
8	0.5	21020	800
9	0.5	21020	1000
10	0.4	29070	250
11	0.6	17220	250
12	0.7	16380	250

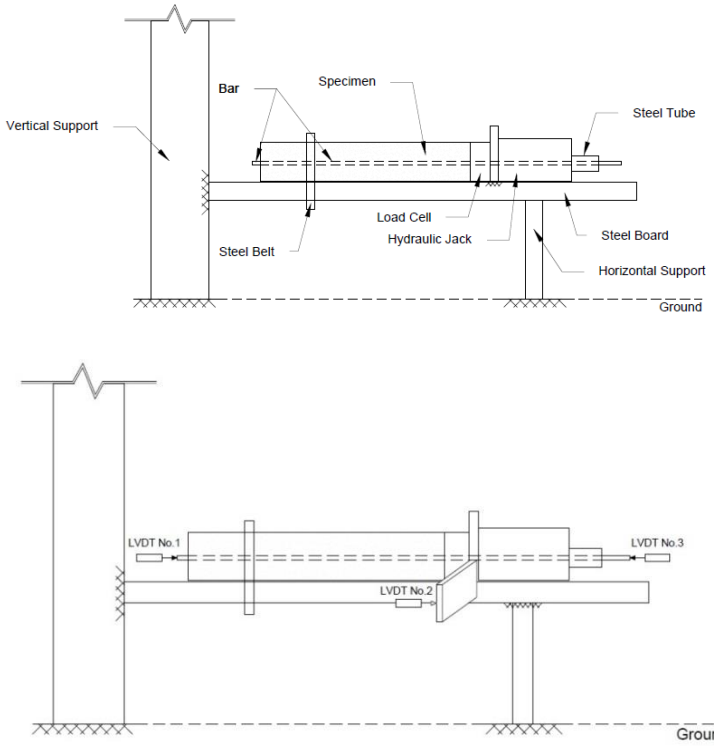

Fig. 1. Pullout test apparatus with no soil surcharge and components.

3.2 Soil box Tests (The Second Series)

The second series of pullout tests were performed in a soil box with a length of 800 mm, width of 520 mm and height of 800 mm. There are two 120-mm-diameter holes on the front and backside of the box for reinforcement installation, which are centered at the level of 340 mm from the top.

Any pullout test in the box includes five layers of soil. For each layer, the required amount of soil was mixed with a specific amount of water and the mixture was poured into the box and was finally

compacted to the desired density. Two vertical pipes, perpendicular to the box longitudinal direction were placed for grouting, one for grouting and the other to ensure that the borehole is completely filled. Table 2 describes the characteristics of pullout tests in the soil box.

Tests No. 13 and 14 have been conducted with a fixed condition of cement grout to reach the ultimate pullout strength of the bar. In other tests, the cement grout could easily move. Details of the pullout soil box and its components are shown in Fig. 2. Also, Fig. 3 describes the details of the tests with fixed cement grout.

To investigate the surcharge pressure effect on the pullout load, four tests with different surcharge pressures including 0, 13, 26 and 40 kN/m^2 have been conducted. Concrete blocks were used to supply the surcharge over the pullout box. Table 3 describes the pullout tests in the soil box under the gravity surcharges.

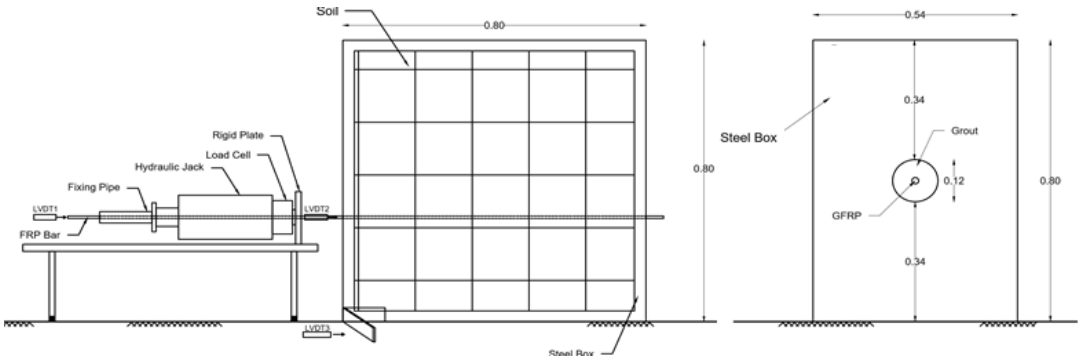

Fig. 2. Details of the pullout tests in the soil box.

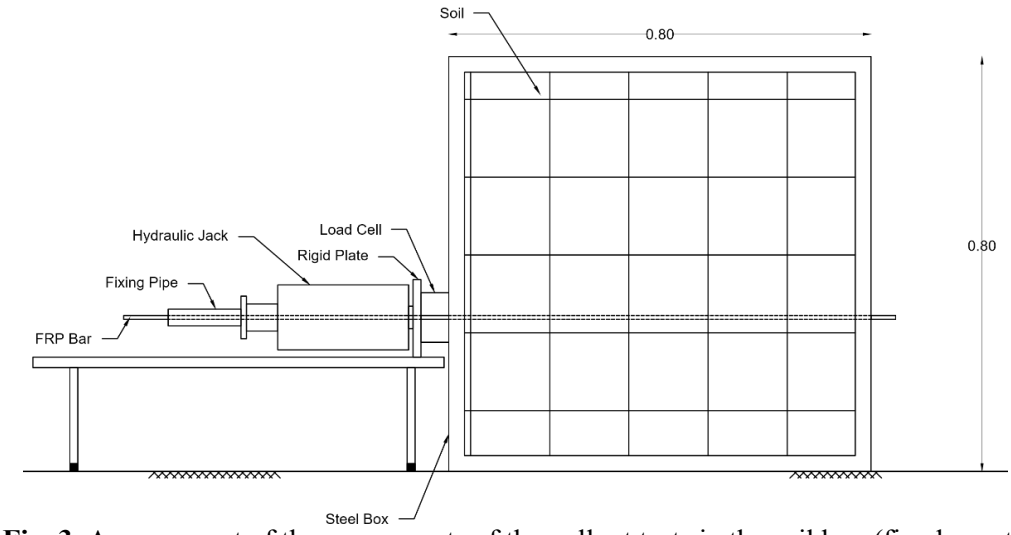

Fig. 3. Arrangement of the components of the pullout tests in the soil box (fixed grout).

Table 2. Tests with different densities of soil surcharge

Test No.	γ_d (kN/m^3)
13	17. 60
14	18.11
15	17.04
16	17.55
17	17.78
18	18.54

Table 3. Tests with surrounding soil and different values of gravity surcharge.

Test No.	γ_d (kN/m^3)	Surcharge Pressure (kPa)
19	17.93	13
20		26
21		40

4. Calibration Process and Results

To investigate the suitability of the models to predict the bond stress between GFRP nails and grout, each model was calibrated using the results of any pullout test separately and the constant parameters were determined. Figures 4-7 show the range of the determined constant parameters of each calibrated model separately.

It should be noted that the proposed values of the parameters by the original developers are examples and are heavily dependent on the properties of the reinforcement and concrete of the actual tests. This is because the values are different. Table 3 compares the calibrated parameters of the bond stresses of GFRP soil nails in two different series with the examples of the parameters of original model developers.

As shown in Table 3, except for one of Malvar model constants (F), the parameters are in shared data intervals. F is about three times less which is most probably due to the diversity of the properties of grout and concrete. There is no particular reason for the similarity of the parameters which have been calibrated by different experiments and conditions, It also may be the reason of differences between the values of the calibrated parameters by original model developers.

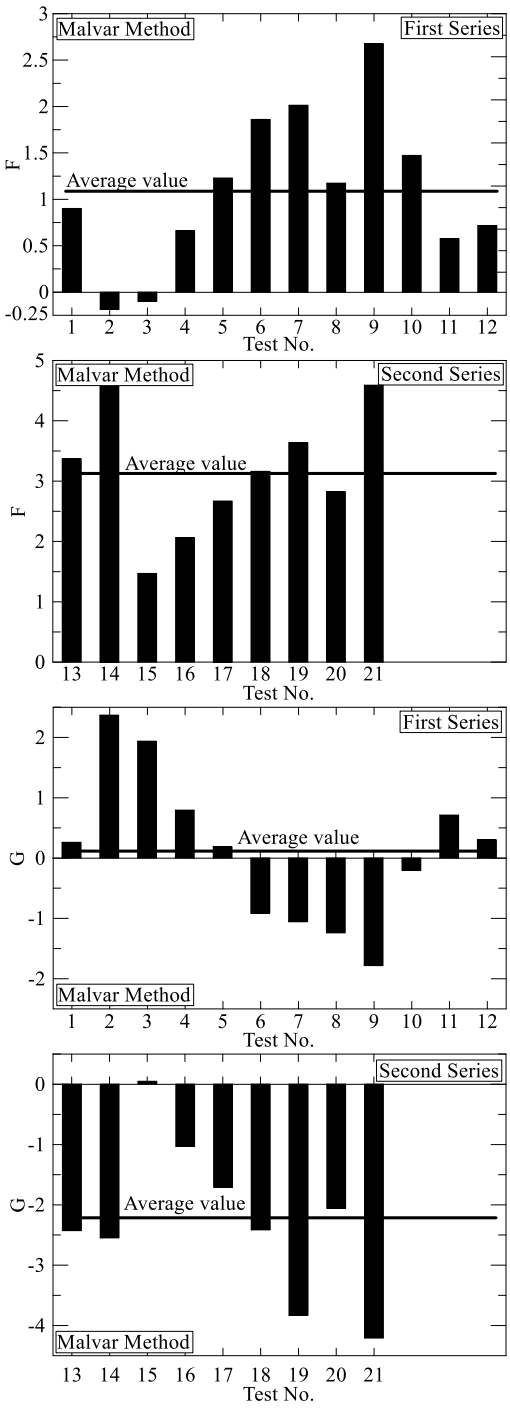

Fig. 4. Variation range of constant parameters in the calibrated Malvar model (F and G).

Table 3. Comparison of the constant parameter range of calibrated and original models.

		GFRP Nail (Research Calibration)	
	Rebar-Concrete (Original Model Developer)	First series	Second series
Malvar, F	F=11.0 and 13.0	F=-0.66 to 2.68	F=1.47 to 4.61
Malvar, G	G=0.50 and 1.20	G=-1.78 to 2.37	G=-4.21 to 0.5
EPB	α=0.33 and 0.45	α=0.37 to 1.23	α=0.36 to 0.67
CMR	α=0.16 to 1.49	α=0.33 to 0.84	α=0.29 to 0.48
Soroushian	-	α=0.88 to 2.11	α=0.94 to 1.40

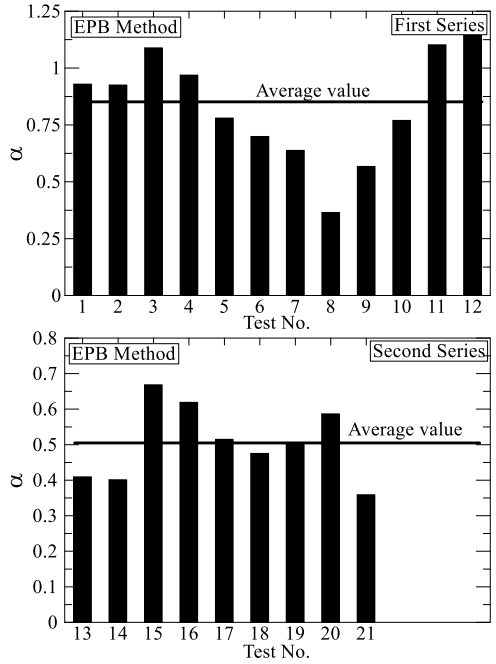

Fig. 5. Variation range of constant parameter in the calibrated EPB model (α).

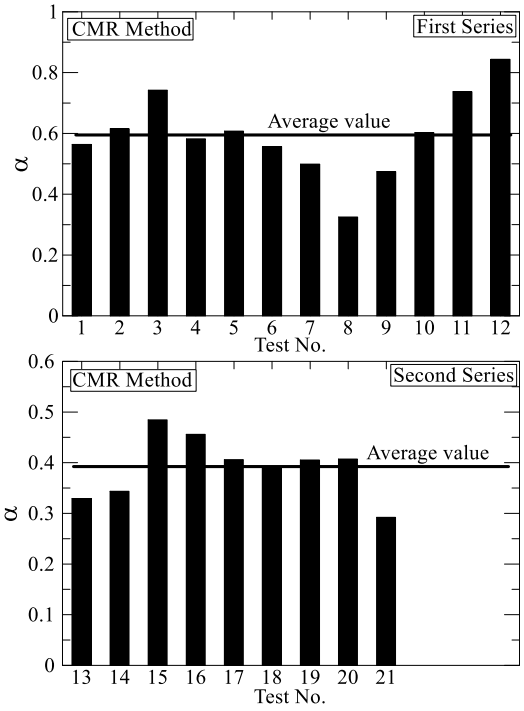

Fig. 6. Variation range of constant parameter in the calibrated CMR model (α).

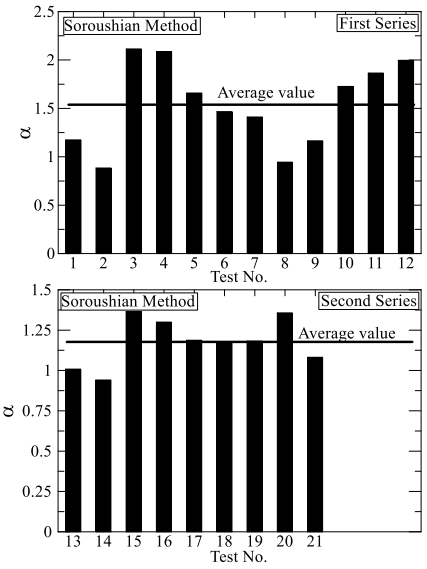

Fig. 7. Variation range of constant parameter in the calibrated Soroushian model (α).

Based on the obtained constant parameters, the bond stress-displacement relationship of each actual test was compared with the calibrated model in a same curve. Figure 8 displays and compares the bond stress-displacement relationships of the actual and calibrated models.

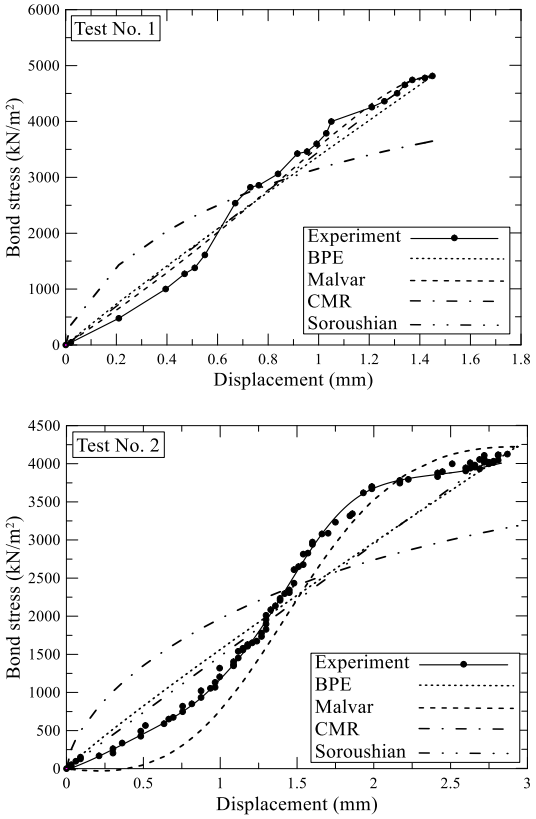

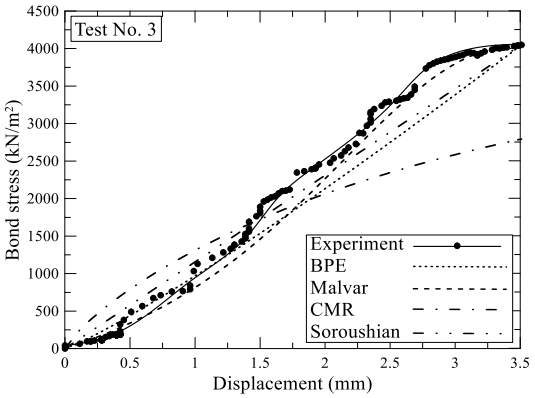
Test No. 3
Bond stress (kN/m²)
Displacement (mm)
Experiment
BPE
Malvar
CMR
Soroushian

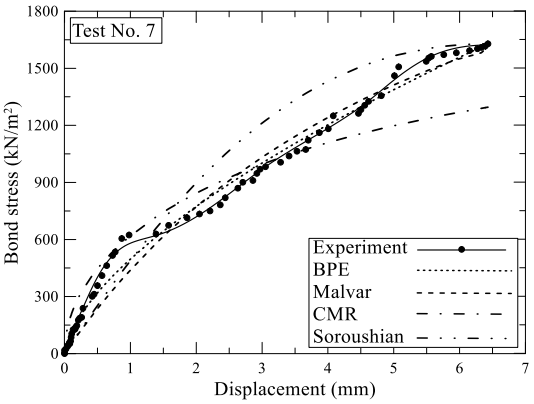
Test No. 7
Bond stress (kN/m²)
Displacement (mm)
Experiment
BPE
Malvar
CMR
Soroushian

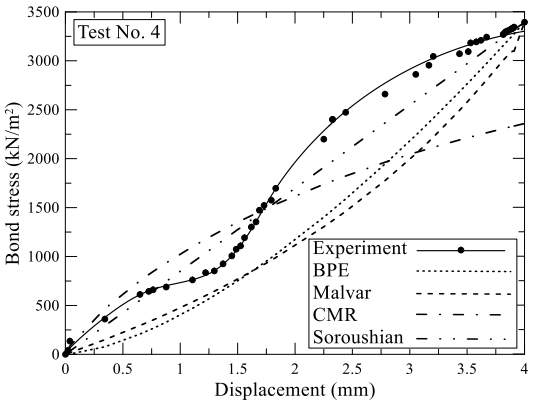
Test No. 4
Bond stress (kN/m²)
Displacement (mm)
Experiment
BPE
Malvar
CMR
Soroushian

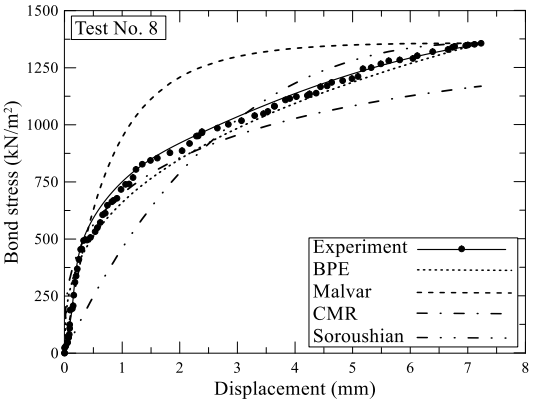
Test No. 8
Bond stress (kN/m²)
Displacement (mm)
Experiment
BPE
Malvar
CMR
Soroushian

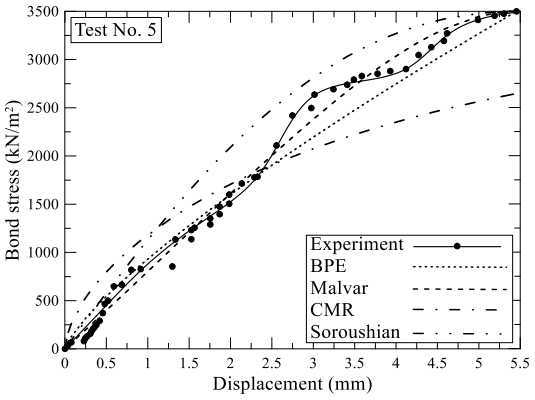
Test No. 5
Bond stress (kN/m²)
Displacement (mm)
Experiment
BPE
Malvar
CMR
Soroushian

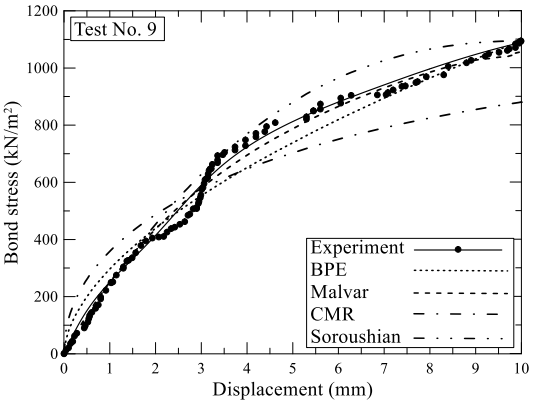
Test No. 9
Bond stress (kN/m²)
Displacement (mm)
Experiment
BPE
Malvar
CMR
Soroushian

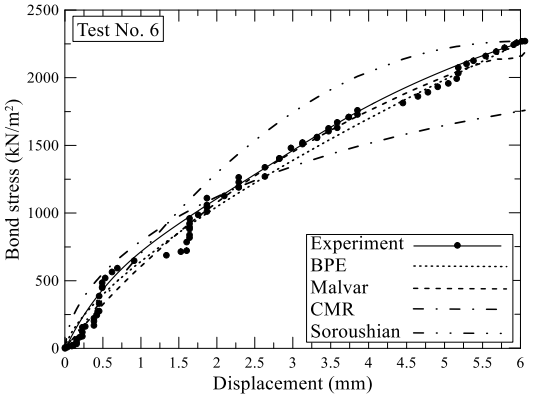
Test No. 6
Bond stress (kN/m²)
Displacement (mm)
Experiment
BPE
Malvar
CMR
Soroushian

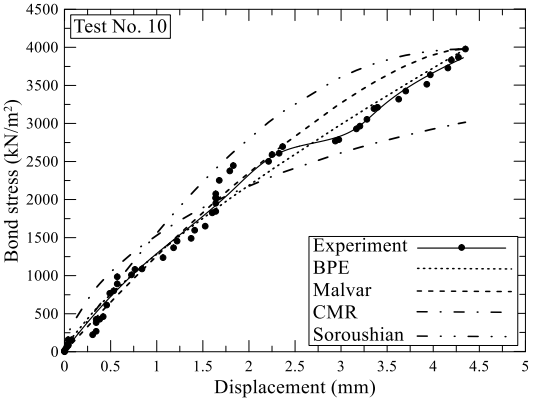
Test No. 10
Bond stress (kN/m²)
Displacement (mm)
Experiment
BPE
Malvar
CMR
Soroushian

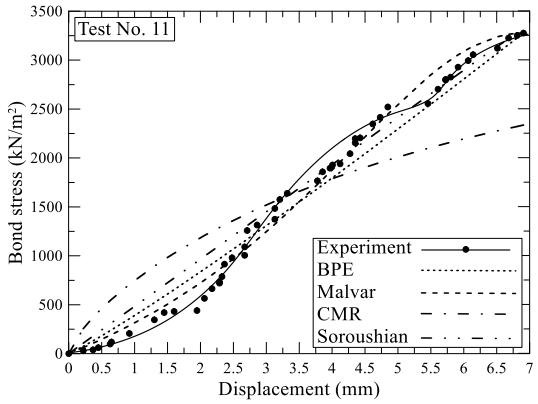
Test No. 11
Bond stress (kN/m²)
Displacement (mm)
Experiment
BPE
Malvar
CMR
Soroushian

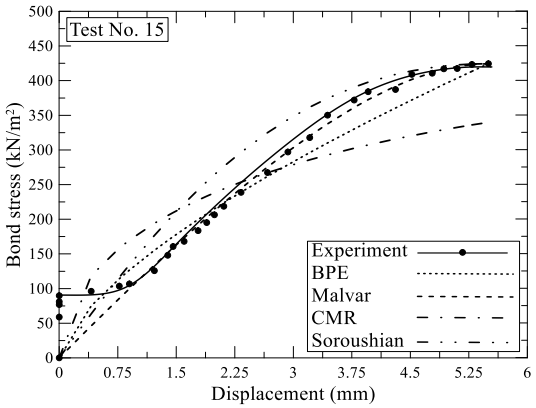
Test No. 15
Bond stress (kN/m²)
Displacement (mm)
Experiment
BPE
Malvar
CMR
Soroushian

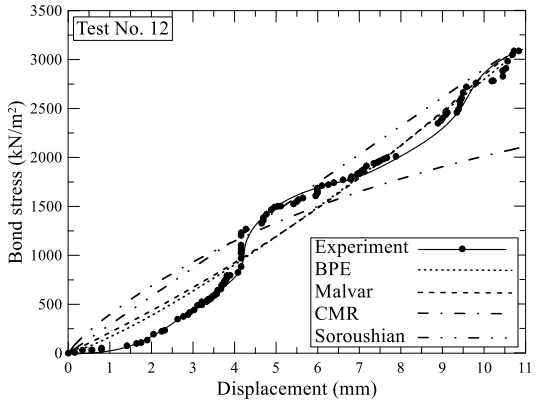
Test No. 12
Bond stress (kN/m²)
Displacement (mm)
Experiment
BPE
Malvar
CMR
Soroushian

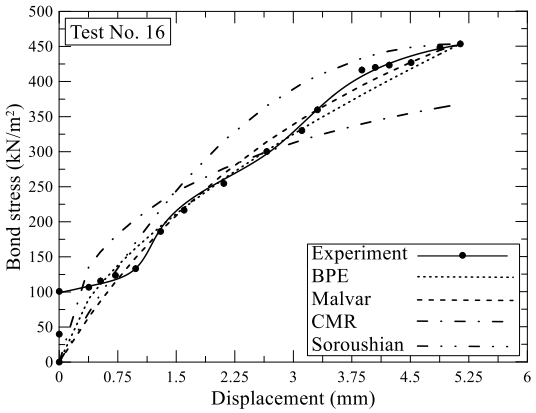
Test No. 16
Bond stress (kN/m²)
Displacement (mm)
Experiment
BPE
Malvar
CMR
Soroushian

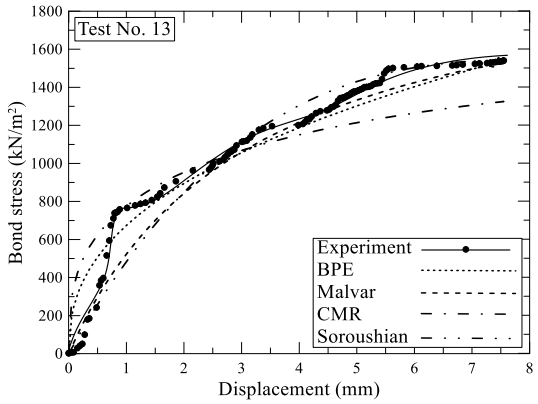
Test No. 13
Bond stress (kN/m²)
Displacement (mm)
Experiment
BPE
Malvar
CMR
Soroushian

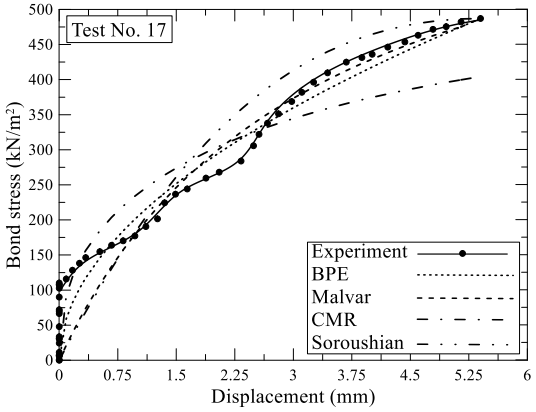
Test No. 17
Bond stress (kN/m²)
Displacement (mm)
Experiment
BPE
Malvar
CMR
Soroushian

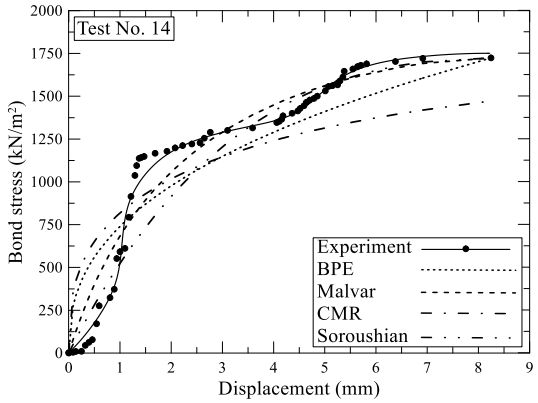
Test No. 14
Bond stress (kN/m²)
Displacement (mm)
Experiment
BPE
Malvar
CMR
Soroushian

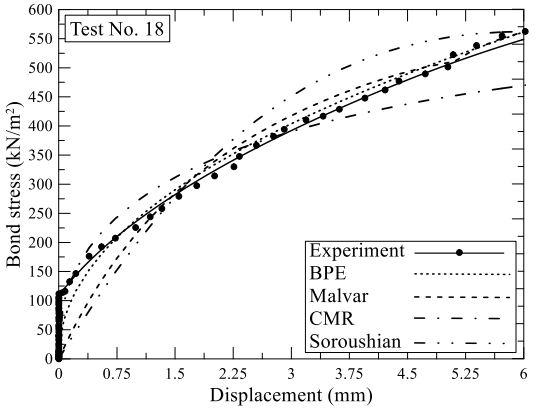
Test No. 18
Bond stress (kN/m²)
Displacement (mm)
Experiment
BPE
Malvar
CMR
Soroushian

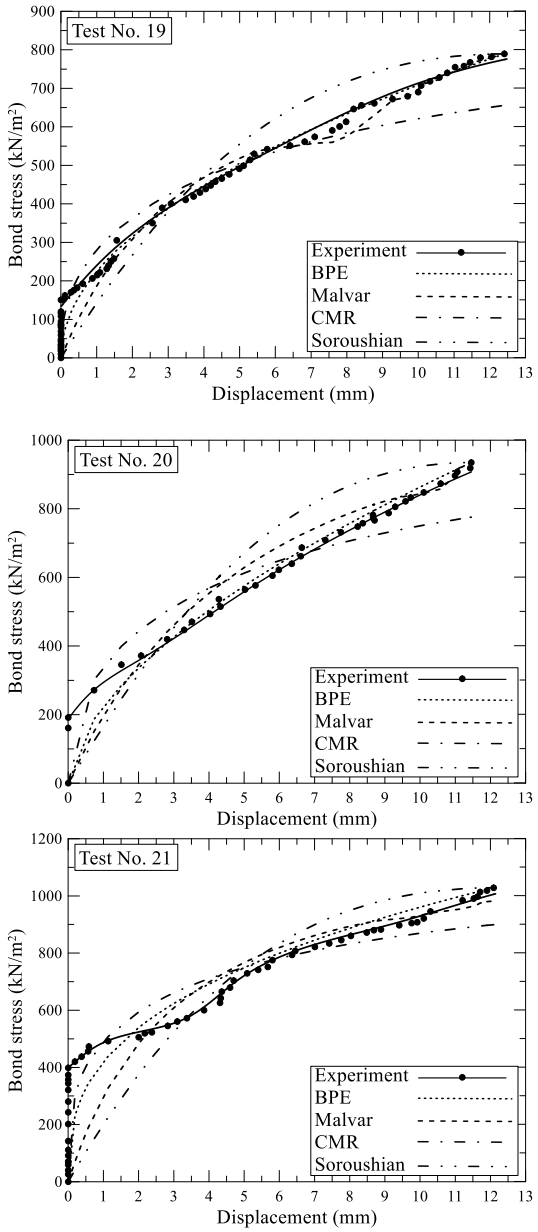

Fig. 8. Comparison of the bond stress-displacement relationships of the actual tests and the calibrated models.

5. Accuracy of the Calibrated Models

Four well-known bond-displacement models of bar-concrete interface have been calibrated for GFRP nails in cement grout and constant parameters determined using the results of experimental pullout tests. To compare the accuracy of the calibrated models, four statistical criteria including R^2, SSE, MAPE and RMSE were determined for any calibration process.

The coefficient of determination, R^2, is interpreted as the proportion of the variance in the dependent variable that is predictable from the independent variable. It means that, the square of the correlations between predicted values by the model and the actual values is called *the coefficient of determination*. R^2 ranges from 0 to 1. The formula to compute the coefficient of determination is given by Eq. (6) [48].

$$R^2 = 1 - \frac{\sum_{i=1}^{N}(y_i - f_i)^2}{\sum_{i=1}^{N}(y_i - \bar{y})^2} \quad (6)$$

In Eq. (7), N, y_i, f_i and $\bar{y}$ signify the number of attempts made to calibrate the model, the y value of the i^{th} attempt, the predicted value by the model and the average value of the observed data, respectively [48].

Sum of squared errors, SSE, can be interpreted as a measure of how much variation in y is left unexplained by the model, $f(x_i)$, or how much cannot be attributed to a linear relationship. It is a measure of the discrepancy between the data and an estimation model. In a model with a single explanatory variable, SSE is given by:

$$SSE = \sum_{i=1}^{n}(y_i - f(x_i))^2 \quad (7)$$

Where the y_i, x_i and $f(x_i)$ signify the i^{th} value of the variable to be predicted, the i^{th} value of the explanatory variable, and the predicted value of y_i, respectively [49].

Root mean square error, RMSE, is the standard deviation of the residuals, while the residuals are a measure of the distance of the data points from the regression line. The RMSE shows how concentrated the data is around the best fit line. Root mean square error is commonly used in different fields to verify the results of the experimental tests. The formula to

determine the root-mean-square-error is described by Eq. (8).

$$RMSE = \sqrt{(f-\sigma)^2} \quad (8)$$

In Eq. (8), f and σ are the predicted value (unknown) and the value observed by attempt (known), respectively [49].

The Mean absolute percentage error (MAPE) is a relative measure, it represents the errors as a percentage of the original data and it is useful for comparing the accuracy of more than one method. In addition, the different ranges of MAPE less than 10%, between 10 and 20%, between 20 and 50% and more than 50% mean an excellent accurate, good, acceptable and inaccurate prediction respectively. The relationship to obtain the MAPE is given by Eq. (9).

$$MAPE = \left[\frac{1}{n}\sum_{i=1}^{n}\left|\frac{\sigma_{ht_i}-\sigma_{hp_i}}{\sigma_{ht_i}}\right|\right]\times 100 \quad (9)$$

In Eq. (9), σ_{ht} and σ_{hp} are the actual known value and the unknown value for prediction, respectively [50].

In order to evaluate the accuracy of the calibrated models, the average value of statistical criteria was determined and compared together. The more the R^2 value approaches unity and the more SSE, MAPE and RMSE values approach zero, the more the accuracy of the models is high.

Table 5 shows the average value of R^2, SSE, RMSE and MAPE for any calibrated model. It can be concluded that for GFRP soil nails in cement grout, Malvar's model would be the best choice (proved by all of the accuracy criteria) while CMR model is not recommendable (based on all of the accuracy criteria). Figures 9-12 shows the graph of the values of the actual tests versus the predicted bond stresses by calibrated models for each model. The accuracy of the calibrated malvar model and the inaccuracy of the calibrated CMR model is again clearly visible. Moreover, performance of EPB model is better than Soroushian.

Table 5. Average values of R^2, SSE and RMSE for calibrated models.

Calibrated Model	R^2	SSE	RMSE	MAPE (%)
Malvar	0.97	0.31	0.07	20.31
EPB	0.95	0.33	0.07	24.90
CMR	0.83	1.40	0.13	34.83
Soroushian	0.93	0.42	0.09	30.74

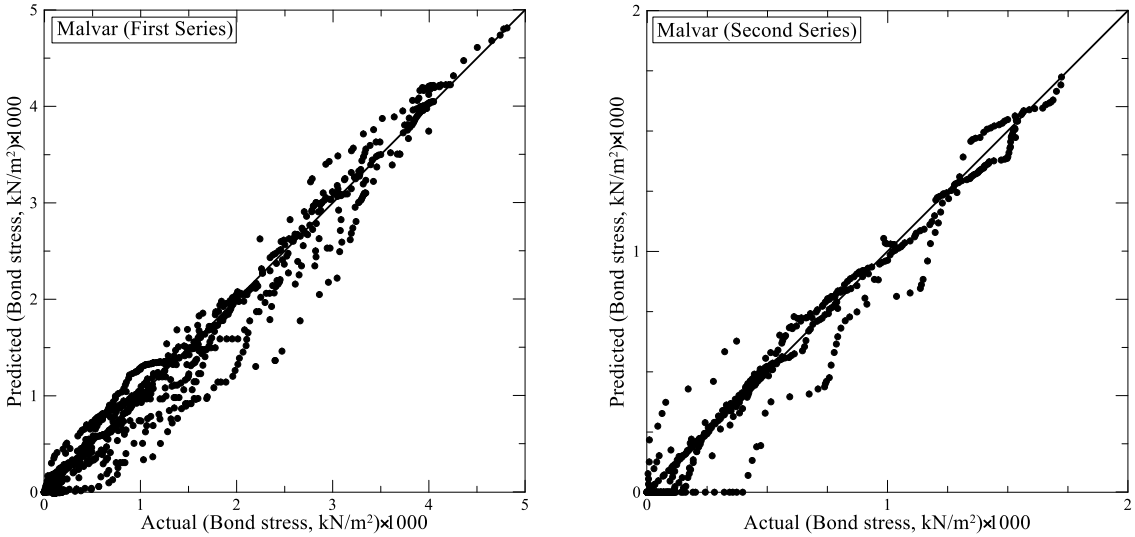

Fig. 9. The bond stresses of actual tests vs. predicted model (calibrated Malvar model).

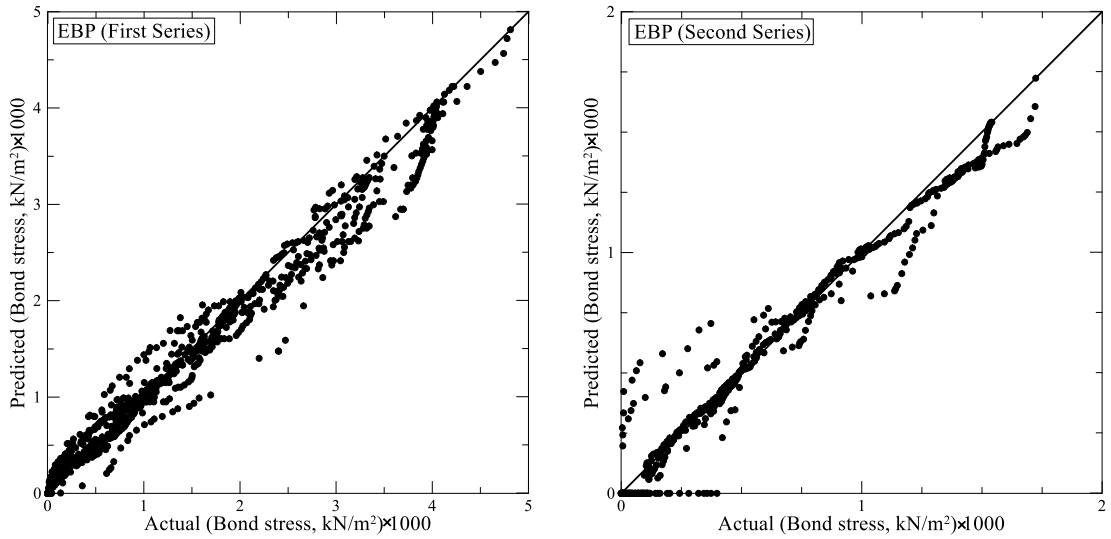

Fig. 10. The bond stresses of actual tests vs. predicted model (calibrated EPB model).

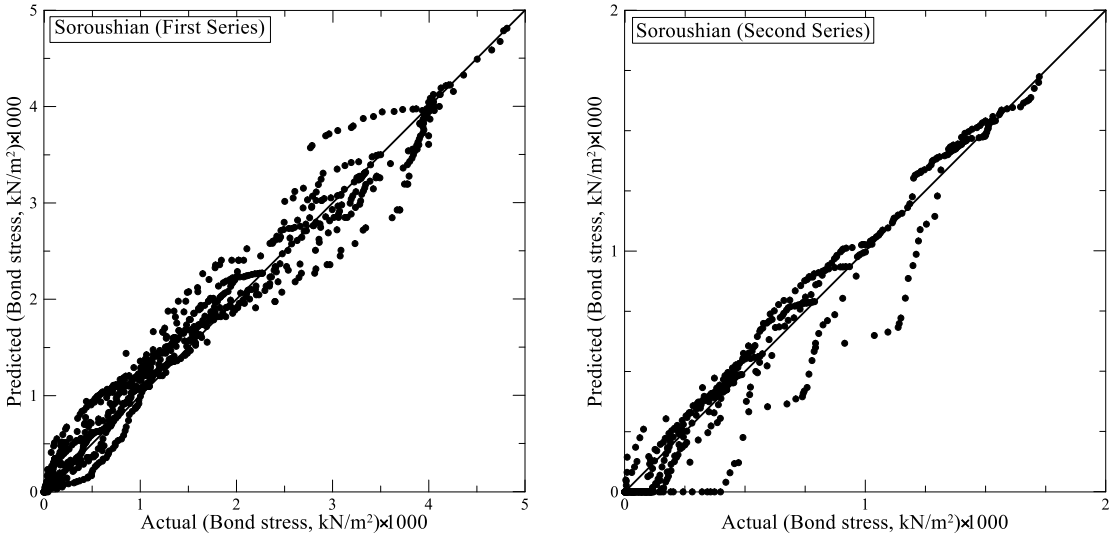

Fig. 11. The bond stresses of actual tests vs. predicted model (calibrated Soroushian model).

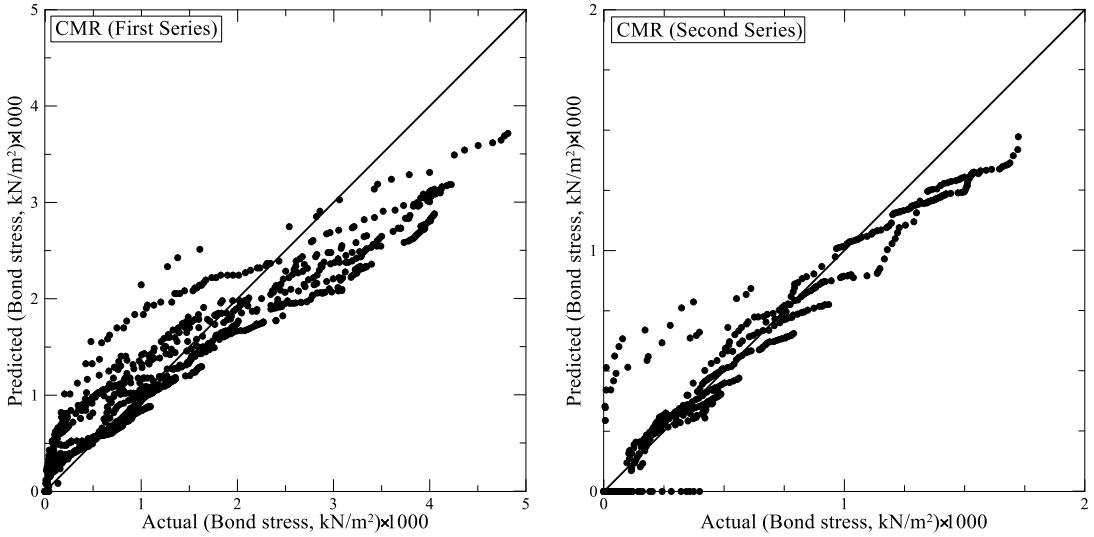

Fig. 12. The bond stresses of actual tests vs. predicted model (calibrated CMR model).

6. Discussion

1. In the first series of the tests, the predicted bond stresses by the calibrated models were more than the values of the actual tests in the first half of the curves (low strains), which is over estimated and should be modified by a suitable factor of safety before designing, otherwise it is not safe. However, in the second half of the curves, all the calibrated models except Soroushian, predicted the bond stress which were less than the actual tests; therefore, it is safe and conservative for designing. Consequently, since the ultimate bond stress (second half) is the main parameter for the design, the calibrated models may be used for design conservatively. Using the Soroushian model is not recommended for predicting the bond stress between GFRP nail and grout.

2. The evaluation of the calibrated models and the actual tests proved that there is an opposite relationship between the accuracy of the calibration and the uniformity of the bond stress distribution. In tests No. 1-9, the uniformity of the bond stress distribution was reduced by increasing the embedded length of GFRP nail. Therefore by rising the embedded lengths, the calibrated models performed more accurately.

3. In the tests No. 10-12, the accuracy of the calibrated models was dropped by decreasing the water cement ratio (an increase of grout compression strength). Therefore, it is recommended to use the ultimate bond stresses with an appropriate safety factor to observe safety.

4. Tests 13 and 14 have been carried out under surrounding soil with fixed grout condition. The accuracy of calibrated models in the first half of the curve (low strains) was not acceptable and the predicted bond stresses were more than the actual tests which would be dangerous in design and practice. However, the models were calibrated with higher accuracy at the second half of the curve (high strains) and the predicted bond stresses including the ultimate bond strength were less than the actual tests, so recommendable for the safe design.

5. In the tests No. 15-21 which both of the grout and the soil could easily move, the calibrated Soroushian model predicted over-estimated bond stress (not safe), calibrated CMR model calculated under-estimated bond stress (costly design), but Malvar and EPB models predicted the ultimate bond strengths less than the experimental tests with high accuracy and good safety. Moreover, the results depicted that as the soil density increased (more compaction), the accuracy of the calibrated models was enhanced.

7. Conclusion

The bond stress between nail and cement grout is one of the main concerns of designers in geotechnical engineering practices. FRP bars as a promising solution for overcoming the corrosion problem have been regarded a good alternative for steel ones. Despite many models to predict

bond stress between rebar and concrete, the studies on bond stress between GFRP nails in cement grout are relatively a few. It was aimed to investigate the reliability of the bond stress models of bar-concrete for predicting the bond stress of GFRP nails. Therefore, four well-known bond stress models were calibrated by the experimental pullout tests of GFRP nails. Also, the accuracy of the calibration process was verified by the statistical criteria. The interesting conclusions of the current research are listed as follows:

1. The calibrated Malvar model demonstrated the best accuracy. Thus, it can be claimed that the calibrated model is capable of predicting the bond stress of GFRP nails in cement grout with desirable accuracy.

2. CMR model did not show a good performance in predicting bond stress of GFRP nails in comparison with others. The original paper of CMR model clearly claimed that the model is heavily dependent on bar surface; therefore, it may be concluded that the CMR model could not predict bond stress of all kinds of GFRP nails with good accuracy.

3. The calibrated Soroushian and EPB models demonstrated fair accuracy for prediction of bond stress of GFRP nails, while they have been originally proposed for bond stress between steel bar and concrete. The evaluation of calibration accuracy also showed a better performance of EPB model than Soroushian to predict bond stresses in GFRP nails.

4. In the tests with different lengths, by increasing the embedded length of GFRP nail, the uniformity of the bond stress distribution was reduced. It was found that there is an inverse relationship between the accuracy of the calibration and the uniformity of the bond stress distribution. By rising the embedded lengths, the calibrated models performed more accurately.

5. The accuracy of the calibrated models was dropped as water cement ratio reduced or grout compression strength increased; therefore, the ultimate bond stress should be used with appropriate safety factors.

6. In the tests with the fixed grout, the predicted bond stress of the calibrated models in the first half of the curve (low strains) was more than the experimental tests. Therefore, it is not secure in practice and it should be used with an appropriate safety factor. However, in higher strains, the predicted bond stresses including the ultimate bond strength were less than the actual tests, thus, they could be recommended for the safe design.

7. In the tests with free to move conditions of grout and soil, the calibrated Soroushian model predicted over-estimated bond stresses with no safety, the calibrated CMR model calculated under-estimated bond stresses which is costly. However, the Malvar and EPB models predicted the ultimate bond strengths less than experimental tests with high accuracy and good safety which are strongly recommended.

REFERENCES

[1] Xu, K., Ren, C., Deng, Q., Jin, Q., Chen, X. (2018). Real-time monitoring of bond slip between GFRP bar and concrete structure using piezoceramic transducer-enabled active sensing, Sensors, 18: 2653.

[2] Zhang, C., Zhou, H., Shi, B., Wu, F., Yin, J. (2015). Experimental investigation of pullout behavior of Fiber-Reinforced Polymer reinforcements in sand, Journal of Composite for Construction, 19: 04014062.

[3] Yan, F., Lin, Z., Wang, X., Azarmi, F., Sobolev, K. (2017). Evaluation and prediction of bond strength of GFRP-bar reinforced concrete using artificial neural network optimized with genetic algorithm, Composite Structures, 161:441-452.

[4] Refai, A., Abed, F., Altalmas, A. (2014). Bond durability of basalt fiber reinforced polymer bars embedded in concrete under direct pullout conditions, Journal of Composites for Construction.

[5] El Refai, A., Ammar, M. A., Masmoudi, R. (2014). Bond performance of basalt fiber-reinforced polymer bars to concrete, Journal of Composites for Construction, 19: 04014050.

[6] Okelo, R., Yuan, R.L. (2005). Bond strength of Fiber Reinforced Polymer rebar in Normal Strength Concrete, Journal of Composites for Construction, 9:203-213.

[7] Özkal, F. M., Polat, M., Yağan, M., Öztürk, M. O. (2018). Mechanical properties and bond strength degradation of GFRP and steel rebars at elevated temperatures, Construction and Building Materials, 184:45-57.

[8] Maranan, G., Manalo, A., Karunasena, K., Benmokrane, B. (2015). Bond stress-slip behavior: case of GFRP bars in Geopolymer concrete, Journal of Materials in Civil Engineering, 27:04014116.

[9] Esfahani, M.R., Rakhshanimehr, M., Mousavi, S.R. (2013). Bond Strength of Lap-Spliced GFRP bars in concrete beams, Journal of Composites for Construction, 17:314-323.

[10] Mostofinejad, D., Mofrad, M. H., Hosseini, A., Mofrad, H. H. (2018). Investigating the effects of concrete compressive strength, CFRP thickness and groove depth on CFRP-concrete bond strength of EBROG joints, Construction and Building Materials, 189:323-337.

[11] Liu, H., Yang, J., Wang, X. (2017). Bond behavior between BFRP bar and recycled aggregate concrete reinforced with basalt fiber, Construction and Building Materials, 135:477-483.

[12] Tekle, B.H., Khennane, A., Kayali, O. (2016). Bond Properties of Sand-Coated GFRP Bars with Fly Ash–Based Geopolymer Concrete, Journal of Composites for Construction, 20:04016025.

[13] Esfahani, M.R., Kianoush, M.R., Lachemi, M. (2005). Bond strength of Glass Fiber Reinforced Polymer reinforcing bars in Normal and Self-Consolidating Concrete, Canadian Journal in Civil Engineering, 32:553-560.

[14] Dong, Z.Q., Wu, G., Xu, Y.Q. (2017). Bond and Flexural Behavior of Sea Sand Concrete Members Reinforced with Hybrid Steel-Composite Bars Presubjected to Wet-Dry Cycles, Journal of Composites for Construction, 21:04016095.

[15] Imjai, T., Guadagnini, M., Pilakoutas, K. (2017). Bond Strength of FRP Bars: Experimental Investigation and Bond Modeling, Journal of Materials in Civil Engineering, 29:04017024.

[16] Bywalski, C., Drzazga, M., Kaminski, M., Kazmierowski, M. (2016). Analysis of calculation methods for bending concrete elements reinforced with FRP bars, Archives of Civil and mechanical Engineering, 16:901-912.

[17] Qeshta, I.M., Shafigh, P., Jumaat, M.Z. (2016). Research progress on the flexural behaviour of externally bonded RC beams, Archives of Civil and mechanical Engineering, 16:982-1003.

[18] Gooranorimi, O., Claure, G., Suaris, W., Nanni, A. (2018). Bond-slip effect in flexural behavior of GFRP RC slabs, Composite Structures, 193:80-86.

[19] Al-Saadi, N. T. K., Mohammed, A., Al-Mahaidi, R. (2018). Bond performance of NSM CFRP strips embedded in concrete using direct pull-out testing with cementitious adhesive made with graphene oxide, Construction and Building Materials, 162:523-533.

[20] Bedon, C., Louter, C. (2018). Numerical investigation on structural glass beams with GFRP-embedded rods, including effects of pre-stress, Composite Structures, 184:650-661.

[21] Carvalho, E.P., Miranda, M.P., Fernandes, D., Victor Alves, G. (2018). Comparison of test methodologies to evaluate steel-concrete bond strength of thin reinforcing bar, Construction and Building Materials, 183:243-252.

[22] Soroushian, P., Choi, K.B. (1989). Local bond of deformed bars with different diameters in confined concrete, ACI Structural Journal, 86:217–222.

[23] Eligehausen, R., Popov, E.P., Bertero, V.V. (1982). Local bond stress-slip relationships of deformed bars under generalized excitations, Earthquake Engineering Research Center, University of California, Berkeley.

[24] Mousavi, S. S., Dehestani, M., Mousavi, K. K. (2017). Bond strength and development length of steel bar in unconfined self-consolidating concrete, Engineering Structures, 131:587-598.

[25] Esfahani, M.R., Kianoush, M.R. (2005). Development/splice length of reinforcing bars, ACI Structural Journal, 102:22-30.

[26] Esfahani, M.R., Rangan, B.V. (1998). Local bond strength of reinforcing bars in Normal Strength and High-Strength Concrete (HSC), ACI Structural Journal, 95:96-105.

[27] Esfahani, M.R., Rangan, B.V. (1998b). Bond between Normal Strength and High-Strength Concrete (HSC) and reinforcing bars in splices in beams, ACI Structural Journal, 95:272-279.

[28] Soroushian, P., Choi, K.B., Park, G.H., Aslani, F. (1991). Bond of deformed bars to concrete: effects of confinement and strength of concrete, ACI Material Journal, 88:227–232.

[29] Abrishami, H., Mitchell, D. (1996). Analysis of bond stress distribution in

pullout specimens, Journal of Structural Engineering, 122:255-261.

[30] Ma, Y., Guo, Z., Wang, L., Zhang, J. (2017). Experimental investigation of corrosion effect on bond behavior between reinforcing bar and concrete, Construction and Building Materials, 152:240-249.

[31] Siamphukdee, K., Zou, R., Collins, F., Shayan, A. (2018). Modeling Steel-Concrete Bond Strength Depletion during Corrosion, ACI Materials Journal, 115.

[32] Yuan, F., Chen, M. (2018). Numerical sensing of plastic hinge regions in concrete beams with hybrid (FRP and steel) bars, Sensors, 18:3255.

[33] Achillides, Z., Pilakoutas, K. (2004). Bond behavior of Fiber Reinforced Polymer bars under direct pullout conditions, Journal of Composites for Construction, 8:173-181.

[34] Tighiouart, B., Benmokrane, B., Gao, D. (1998). Investigation of bond in concrete member with fiber reinforced polymer (FRP) bars, Construction and Building Materials, 12:453-462.

[35] Yu, S., Zhu, W., Niu, L., Zhou, S., Kang, P. (2019). Experimental and numerical analysis of fully grouted long rockbolt load-transfer behavior, Tunnelling and Underground Space Technology, 85:56-66.

[36] Liu, H., Tang, L., Lin, P. (2018). Estimation of ultimate bond strength for soil nails in clayey soils using maximum likelihood method, Georisk: Assessment and Management of Risk for Engineered Systems and Geohazards, 12:190-202.

[37] Dybel, P., Furtak, K. (2016). The effect of ribbed reinforcing bars location on their bond with high-performance concrete, Archives of Civil and mechanical Engineering, 15:1070-1077.

[38] Seo, H.J. Jeong, K.H., Choi, H., Lee, I.M. (2012). Pullout resistance increase of soil nailing induced by pressurized grouting, Journal of Geotechnical and Geoenvironmental Engineering, 138:604-613.

[39] Lee, S.W., Kim, T.S., Sim, B.K., Kim, J.S., Lee, I.M. (2012). Effect of pressurized grouting on pullout resistance and group efficiency of compression ground anchor, Canadian Geotechnical Journal, 49:939-953.

[40] Su, L.J., Yin, J.H., Zhou, W.H. (2010). Influences of overburden pressure and soil dilation on soil nail pull-out resistance, Computers and Geotechnics, 37:555-564.

[41] Xu, D. S., Liu, H. B., Luo, W. L. (2018). Evaluation of interface shear behavior of GFRP soil nails with a strain-transfer model and distributed fiber-optic sensors, Computers and Geotechnics, 95:180-190.

[42] Zhang, B., Benmokrane, B., Ebead, U.A. (2006). Design and evaluation of Fiber-Reinforced Polymer bond-type anchorages and ground anchors, International Journal of Geomechanics, 6:166-175.

[43] Zou, W.L., Wang, X.Q., Vanapalli, K. (2016). Experimental evaluation of engineering properties of GFRP screw anchors for anchoring applications, Journal of Materials in Civil Engineering, 28:04016029.

[44] Kou, H.l., Guo, W., Zhang, M.Y. (2015). Pullout performance of GFRP anti-floating anchor in weathered soil,

Tunneling and underground space technology, 49:408-416.

[45] Zheng, J.J., Dai, J.G. (2014). Analytical solution for the full-range pull-out behavior of FRP ground anchors, Construction and Building materials, 58: 129-137.

[46] Malvar, LJ. (1994). Bond stress-slip characteristics of FRP rebar, Naval Facilities Engineering Service Center, California.

[47] Cosenza, E., Manfredi, G., Realfonzo, R. (1995). Analytical modelling of bond between FRP reinforcing bars and concrete, In: Nonmetallic (FRP) reinforcement for concrete structures, E&FN Spon, London, 164–171.

[48] Devore, J.L. (2011). Probability and Statistics for Engineering and the Sciences, Cengage Learning, 8th edition, Boston.

[49] Barnston, A. (1992). Correspondence among the Correlation [root mean square error] and Heidke Verification Measures; Refinement of the Heidke Score, Notes and Correspondence, Climate Analysis Center.

[50] Gnananandarao, T., Dutta, R. K., Khatri, V. N. (2019). Application of Artificial Neural Network to Predict the Settlement of Shallow Foundations on Cohesionless Soils, Geotechnical Applications, 13:51-58